A BAYESIAN FORMULATION OF GRAPH-CUT SURFACE ESTIMATION WITH GLOBAL SHAPE PRIORS

Gopalkrishna Veni[1], *Shireen Y. Elhabian*[1,2], *Ross T. Whitaker*[1]

[1] Scientific Computing and Imaging (SCI) Institute, University of Utah, USA
[2] Faculty of Computers and Information, Cairo University, Egypt

ABSTRACT

In this paper, we propose a formulation of graph-cut segmentation that relies on a generative image model by incorporating both local and global shape priors. With surface estimation, rather than pixel classification, we cast the segmentation problem as a maximum *a posteriori* estimation from the image intensities via a *cut* through a multi-layer three-dimensional mesh model that preserves the topology of the shape class of interest. Methods that rely on local optimization techniques and/or local shape penalties, e.g., smoothness, have been proven to be ineffective to address challenging segmentation problems, such as noisy/ill-defined boundaries and irregular shapes. On the other hand, our method relies on graph cuts as well as a new formulation to estimate shape parameters in a closed form that provides a global updates-based optimization strategy. We demonstrate our formulation on synthetic datasets as well as the left atrial wall segmentation from late-gadolinium enhancement MRI, which is useful in atrial fibrillation to identify fibrosis, but presents local contrast and noise within the wall.

Index Terms— Bayesian Segmentation, Atrial Fibrillation, Minimum *s-t* Cut, Mesh Generation, Geometric Graph.

1. INTRODUCTION

Accurate segmentation of medical images is a ubiquitous demand in clinical studies for diagnosis and analysis. Nonetheless, specific classes of organs/tissues present a challenging combination of features including heterogeneous pixel intensities, noisy diffuse boundary features and irregular shapes, which often arise during the soft tissue imaging for a variety of applications in neuroscience/neurology, cardiology and oncology, to name a few. One such challenge is the segmentation of the left atrium (LA) wall from late-gadolinium enhancement cardiac MRI (LGE-MRI) in patients suffering from atrial fibrillation (AF). LA wall segmentation is crucial to characterize fibrosis (tissue remodeling) in patients prior to radiofrequency ablation therapy (pre-ablation) and for follow-up studies of LA wall scarring in patients after radiofrequency ablation (post-ablation) [1]. Examples of such images are shown in Figure 1a.

Weak boundary segmentation problems are often solvable only if one has some *a priori* notion of shapes in question; motivating a Bayesian framework for segmentation being cast as a surface estimation problem. In the extreme case, one might restrict the solution to some low-dimensional set of shapes defined through training data, as is done with *active shape models* (ASM) [2], active appearance models (AAM) [3] and many variations derived from these approaches. Nonetheless, segmentations must follow correct boundaries rather closely, and yet coarsely similar to a reasonable summary of the training dataset. Furthermore, many surface-based approaches rely on some type of incremental fitting algorithm, such as gradient descent, which is prone to get trapped in local minima, especially if one allows for a very expressive prior to accurately capture details. Based on learning the topology from the shape prior paradigm, our work is built on the ASM approach by projecting onto a low-dimensional, statistical description from a set of training shapes/images. However, the proposed method also accommodates shapes that are not represented in this low-dimensional description. Thus, the method offers optimization schemes that do not rely on incremental updates to shapes or parameters, as is the case of a gradient descent scheme.

Graph cut methods, on the other hand, have recently been extended to incorporate shape priors. For example, [4, 5] rely on the variations of *pixel labeling* formulation for the graph-cut segmentation of Boykov and Jolly [6]. The idea is to identify pixels based on the specified intensity distributions, and then project those pixel classifications onto shape priors, so that the priors affect pixel classification probabilities. The optimization schemes are quite effective, but still approximate. In [7], Gorelick *et al.* use an approximate model to minimize segmentation energies but their method is designed for single surface, which does not fit our application. To address multi-surface segmentation, [8] and [9] rely on intensity or statistical differences across boundaries. Although surface-separation constraints are enforced, they do not use soft penalties with preferred separation distance, and thus their approaches suffer from extracting irregular surfaces. Moreover, no parametrized shape priors are embedded in their graph-structure. Such priors are necessary for weak boundary segmentation problems. Further, [9] uses an approximation graph-cuts scheme that converges to a locally optimal solution while reconstructing the entire graph during each iteration.

The proposed framework builds on the work related to the optimal net surfaces [10] and their applications to medical image segmentation [11, 12]. The segmentation problem is specified as an optimal net surface through a proper ordered (PO) graph, where that net is defined by a minimum *s-excess* set and reduced to a minimum *s-t* cut, for which a global solution is efficient. Veni *et al.* [13] used this surface-net approach to solve for a similar problem. However, they do not incorporate any shape information which, we believe, is essential while dealing with low quality images accompanied with ill-defined boundaries. Song et al. [12] introduced shape priors into such a surface estimation scheme, but the priors were strictly local, implemented as modifications to smoothness parameters in the optimal cut formulation. Here we propose a surface-based segmentation algorithm that relies on a fully generative model that incorporates a global shape prior, controlled smooth deviations from that prior and a combination of a linear system and graph-cut approach

The authors would like to acknowledge Josh Cates, the CARMA Center, CIBC by NIH Grant P41 GM103545-14 and NAMIC through NIH Grant U54 EB005149, for providing Utah fibrosis data.

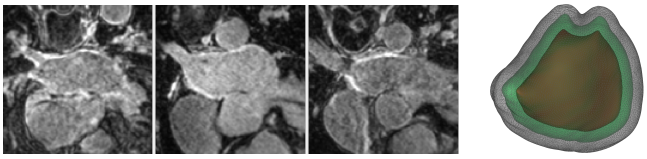

(a) (b)

Fig. 1. (a) Slices of left atrium DE-MRI images showing the challenges in segmentation. (b) An example of several layers of a PO-mesh for the LA

to maximize *a posteriori* optimization. Thus, the resulting optimal segmentation not only is based on the prior but also accommodates irregularities in the test data in order to best match image intensities. Moreover, we estimate the shape parameters, in closed form, for segmentation as a part of the optimization process.

2. METHODOLOGY

2.1. Bayesian Formulation

We begin by defining a segmentation $\mathcal{S}$ as a surface whose vertices are defined on a 3D grid and are connected by edges that form a triangular mesh. Associated with each vertex is an intensity profile (e.g., a 3D patch or a 1D array of intensities) oriented along the approximate normal to the surface, as in [13]. Thus, a particular surface induces a probability on a set of image intensities near each point on the surface. The segmentation takes place on a set of columns, which are connected via a triangular mesh structure as described in [13]. Each column has a set of 3D vertices along its length. Thus, the columns span the 3D space in which the segmentation takes place, as seen in Figure 1b. A particular vertex at the jth position along ith column has a 3D position x_{ij}. The graph has M columns and N vertices along each column. In principle, this column set is a discrete approximation of an underlying continuous parametrization of a subset of $\Re^3$ that relies on surface integrals within which the surface estimation takes place. This *parametrization* also defines the topology of the resulting segmentation. For simplicity, we present only the discrete formulation. A segmentation $\mathcal{S}$ is the set of nodes $\{s(i) \in [1, N]\}\, \forall i \in [1, M]$ representing the position of the surface.

We use a Bayesian formulation to express the posterior probability of a segmentation $\mathcal{S}$ and underlying shape parameters β as a function of the full image I.

$$P(\mathcal{S}, \beta|I) \propto P(I|\mathcal{S}, \beta)P(\mathcal{S}, \beta) = P(I|\mathcal{S}, \beta)P(\mathcal{S}|\beta)P(\beta). \quad (1)$$

$P(I|\mathcal{S}, \beta)$ is a generative model of intensities in the vicinity of a segmentation. We use a Gaussian distribution centered around a mean intensity profile, μ_i, at each point on the associated surface, where μ_i for column i is estimated from the training data. We consider the set of intensities[1] p_{ij} at a vertex x_{ij} to be statistically independent from one vertex to another, which results in a product of probabilities and a sum for the log of the conditional probability.

$$-\log P(I|\mathcal{S}, \beta) = \frac{1}{2\sigma_I^2} \sum_i ||p_{i,s(i)} - \mu_i||^2 \quad (2)$$

$P(\mathcal{S}|\beta)$ describes the probability of a surface estimate as a function of the shape parameters. We represent the surface as a base shape $\mathcal{S}_\beta$ and an offset $\mathcal{S}_o$ where $\mathcal{S} = \mathcal{S}_\beta + \mathcal{S}_o$. For a given set of shape parameters β, the surface probability depends only on the offset, which needs to be small (the shape should be similar to the base shape) and smooth (nearby columns should have similar offsets). Therefore the log-probability can be written as:

$$-\log P(\mathcal{S}|\beta) = \frac{1}{2\sigma_o^2} \sum_i s_o^2(i) + \frac{1}{2\sigma_\mathcal{C}^2} \sum_{(i,j)\in\mathcal{C}} \left(s_o(i) - s_o(j)\right)^2. \quad (3)$$

where σ_o and $\sigma_\mathcal{C}$ are standard deviations of surface offsets learned from the training set and the neighborhood structure, defined by $\mathcal{C}$, which is the clique in the base graph defined over the base shape.

For the shape parameters, we use PCA on a set of distance transforms (DT) of the training data [14], and choose a low-dimensional subspace that maintains 97% of data variability to represent the prior. The Gaussian model for the shape space gives:

$$-\log P(\beta) = \frac{1}{2}\beta^T \Lambda^{-1} \beta, \quad (4)$$

where β is a vector of shape parameters and Λ is the diagonal matrix of eigenvalues from the PCA. The eigenvectors (eigen DT) d_{e_k} from PCA, along with the shape parameters β, are used to construct the corresponding DT d_β.

$$d_\beta(x) = d_\mu(x) + \sum_k \beta_k d_{e_k}(x), \quad (5)$$

where $x \in \Re^3$ and d_μ denotes the mean DT. We use d_β to express the conditional surface probabilities in (3). The DT for a particular β plays two roles. For a given β, we can build the surface $\mathcal{S}_\beta$ by computing the intersection of each column i with the zero crossing of d_β, to give a vertex and 3D positions for $s_\beta(i)$. The DT also gives a convenient way to compute the penalty on the magnitude of the offset from $\mathcal{S}_\beta$, which becomes $\sum_i d_\beta^2(s_i)$, where $s_i = x_{s(i)}$, the sum of square distances of the cuts along each column i from the β-shape.

Thus, we have a full, shape-based generative model of an image. A point β in the low-dimensional shape space, derived from PCA on training data, chosen from a multivariate normal distribution, gives rise to a DT, whose zero level set is the β-shape $\mathcal{S}_\beta$. An offset from this β-shape is chosen from a distribution defined by a Markov random field (MRF) model that favors smaller yet smoother offsets. Notice, this offset model extends the learned probability distribution from the low-dimensional PCA subspace into the entire shape space in a way that favors smooth shapes that are very near, but do not exactly resemble, the training set. Finally, each point on that surface gives rise to an array (patch or vector) of image intensities that are drawn from (identically, independently) a Gaussian distribution, with a mean and covariance that are learned from the training data along each column.

It is worth noting that the LA wall segmentation problem consists of a pair of nested surfaces (epicardium and endocardium). Thus, the above formulation is applied such that the distance transforms are modeled jointly. Similar to [13], we introduce a penalty on the inter-surface distances (expressed in the same probabilistic framework, learned from the data and tied to the β-shape-pair) such that the surfaces are estimated optimally in a joint formulation.

2.2. Optimization

We present a global optimization solution by following an alternating scheme in which we iterate between two fast *global* optimization phases on two sets of parameters.

In the first phase, we optimize for $\mathcal{S}$ given β where we use graph cuts to solve the VCE-weight net surface problem using [10]. We use the MRF formulation [13], which is related to the derivation introduced in [15]. The basic strategy is to express the above penalties

[1] This set of intensities could be organized in any way around a node on the mesh, but for this work we use a 1D array, a kind of *stick* configuration, which is shown in Figure 2a.

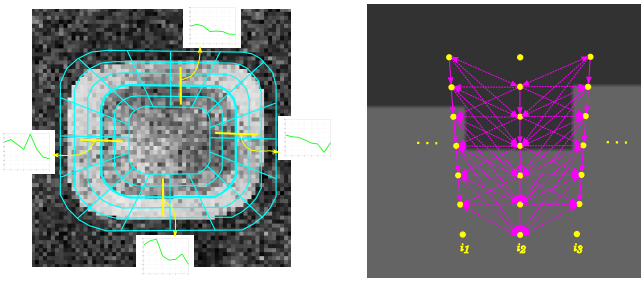

(a) (b)

Fig. 2. (a) 2D illustration of a simplified PO-mesh and *sticks* (yellow) at different mesh points, (b) Arc construction between adjacent columns with respect to $\mathcal{S}_\beta$

as a set of weights on vertices and edges of a PO-graph and reduce the surface estimation problem to a *s-excess* cut on the graph. The *s-excess* cut produces an optimal low-order polynomial time solution– and in practice runs very fast, even on large graphs. The details of the graph construction follow from [10] with some modifications, and therefore we give a high-level view of the algorithm here.

Weights/costs on the graph vertices arise from two sources: (1) a matching term in the image probability, by sampling image patches around each vertex and comparing them against the learned mean, and (2) sampling the squared DT of the β-shape at each vertex position. These terms are weighted and added to generate vertex costs. Edges are inserted along graph-columns and also between the nodes of adjacent columns. The inter-column edges model the pairwise clique potential $C(s_i, s_j)$, associated with the offsets, rather than the absolute positions of the surface, as in previous work. For the optimization to be feasible, we use $C(d) = \alpha d^2$, where $d = (s_i - s_j)$. The β-shape $\mathcal{S}_\beta$ gives a position on each column and $\mathcal{S}_o$ is computed with respect to $\mathcal{S}_\beta$. Thus, the inter-column arcs are adjusted, relative to the $\mathcal{S}_\beta$. Figure 2b summarizes the graph construction of the above configuration of intra- and inter-column arcs. The resulting graph on which we estimate the cut becomes a numerical construct and does not define or heavily influence the shapes of the objects to be segmented. If a mesh is sufficiently fine grained, it only serves to restrict the topology of the surface. The $\mathcal{S}_\beta$ defines an arbitrary surface through the mesh and the offsets allow smooth perturbations on that shape. For a given β, the surface estimate $\mathcal{S}$, computed using the graph-cut, is the global optimum of the posterior in (1).

In the second phase we optimize for β in a closed form given a segmentation $\mathcal{S}$. Here we take the derivative of the log posterior with respect to β and equate it to zero.

$$\frac{1}{\sigma_o^2}\sum_i d_\beta(s_i)\frac{\partial d_\beta}{\partial \beta}(s_i) + \Lambda^{-1}\bar{\beta} + \frac{1}{\sigma_c^2}\sum_{(i,j)}\left(d_\beta(s_i) - d_\beta(s_j)\right)\left(\frac{\partial d_\beta}{\partial \beta}(s_i) - \frac{\partial d_\beta}{\partial \beta}(s_j)\right) = 0. \quad (6)$$

From (5), d_β is a weighted sum of images. The images $\partial d_\beta/\partial\beta$ are the principle components (eigen DT) from the PCA decomposition of the distance transforms in the training set. By isolating β in (6), we obtain a closed-form algebraic solution on vectors/matrices in the space of shape parameters.

$$\bar{\beta} = -(\sigma_c^2 P^a + \sigma_o^2\sigma_c^2\Lambda^{-1} + 2\sigma_o^2(P^a - P^b))^{-1} \times (\sigma_c^2 q^a + 2\sigma_o^2(q^a - q^b)) \quad (7)$$

$$q_k^a = {d_\mu}^T d_{e_k}, \text{and} \quad q_k^b = {d_\mu}^T \mathcal{C}_\mathcal{N} d_{e_k} \quad (8)$$

$$P_{kl}^a = {d_{e_k}}^T d_{e_l}, \text{and} \quad P_{kl}^b = d_{e_k}\mathcal{C}_\mathcal{N} d_{e_l}. \quad (9)$$

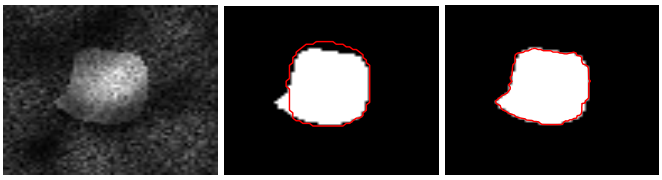

Fig. 3. Left: the original image. Middle: Boykov's result overlaid on the ground-truth segmentation. Right: Our result.

where $\mathcal{C}_\mathcal{N}$ represents the $M \times M$ indicator matrix, with its elements equal to 1 if $j \in \mathcal{N}_i$ (neighborhood of i), else 0. This is the *optimal* β for a given surface segmentation, which finds a compromise between fitting the current segmentation and choosing a likely β based on the Gaussian distribution.

When we consider the algorithm in full, this method differs significantly from others that, in general, either work strictly within the shape space [2] or project intermediate solutions onto that subspace. Here, the optimization strategy offers two advantages. First, it allows intermediate results to deviate from the low-dimensional shape space and to pull the βs along. Second, in each iteration we perform a global optimization of $\mathcal{S}$ and β, thus relying less on local image properties near the current solution. Thus, the algorithm converges with relatively few iterations.

3. EXPERIMENTS AND RESULTS

In order to make a reasonable comparison of our approach with the state-of-art graph-cut algorithms including Boykov's, we considered 2D superquadric examples, corrupted with Rician noise and a smoothly varying bias field. The corresponding energy function to be minimized is given by [6]:

$$E = E_{Data} + E_{Smooth} = \sum_{p\in\mathcal{P}} D_p(x_p) + \sum_{(p,q)\in\mathcal{C}} V_{p,q}(x_p, x_q). \quad (10)$$

The data costs were computed with respect to the mean DT of the training set and the smoothness costs were computed as the normalized cross correlation between the intensity profile at each point and the corresponding model profile that was again derived from the training set. Figure 3 shows the effect of weights on data and smoothness terms, and the corresponding result using our approach. Such incorrect object delineation in Boykov's case is due to the absence of the shape prior, lack of well-defined smoothness structure that is derived from the MRF property and incompetence of allowing only one *cut* per column.

To evaluate our framework, we applied it to 100 simulated images (64×64×96 voxels) and 58 clinical LGE-MRI (29 pre- and 29 post-ablation, 400×400×107) images that were obtained retrospectively from an AF patient image database at the University of Utah's Comprehensive Arrhythmia Research and Management (CARMA) Center. Based on the capture range of two surfaces, 50 mesh layers were used for simulated data and 30 layers were generated for LA examples. We used the dynamic particle system to generate the initial mesh and respective layers (see [13] for details). The mesh does not get rebuilt during segmentation as it has enough layers and resolution to allow shape flexibility. It is the cut through the mesh that is modified to embed shape parameters.

For a given test example, the algorithm relies on the user input to locate its approximate center based on which the nested-mesh is positioned. The algorithm is robust enough as long as the mesh does not lie either outside or inside the desired surface. The input image is sampled along all sticks at all nodes. Next, the posterior probability is computed using (1) which reflects the assignment of

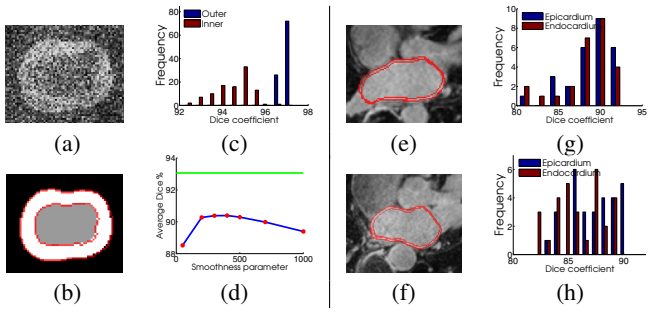

Fig. 4. (a) 2D slice of a perturbed, noisy synthetic example, (b) Segmentation boundaries overlaid on ground-truth (c,g,h) dice histograms of two surfaces on synthetic, pre- and post-ablation datasets (d) Average dice comparison of our method (green) vs VCEnet without shape priors for different α (e) LA wall 1 (f) LA wall 2

costs, weights, edge capacities and then an optimal cut. A pair of optimal mesh surfaces is then recovered from the minimum *s-t* cut. Using this *cut*, the shape parameters are optimized. This procedure is repeated until (1) converges[2]. Based on the extracted topological mesh structure defined by the final cut, it is scan-converted to reproduce segmented volume(s). The scaling parameter α for the potential function C is fixed to 300 for the synthetic case and 100 for the LA dataset. These values reflect the complexity of surfaces.

For the simulated data, we considered 30 training examples and 100 test cases, which include two oblong mutually interacting surfaces. To mimic the variations of the LA-wall thickness, we incorporated shape changes by perturbing both of the surfaces in each image by means of a randomly (Gaussian distributed with $\mu = 11$, $\sigma^2 = 36$) corrupted DT to generate wiggles on the surfaces. Next, each image was corrupted with Rician noise (with $\sigma = 30$) and a smoothly varying bias field (see, e.g., Figure 4a). Figure 4b shows our segmentation result on the corresponding ground-truth to prove the effectiveness of our approach in retrieving both the boundaries correctly, even in such a challenging environment.

For the quantitative evaluation, we used the Dice metric to analyze the overlapping percentage between our segmentation result and the ground-truth. Figure 4c shows the histogram plot of Dice measures on both surfaces. To prove the effectiveness of embedding global shape priors into the VCE-weight net framework, we compared the average Dice of the middle layer over all images to the one that does not include the prior. As shown in Figure 4d, the average Dice percentage with the shape prior is 93.06%. By contrast, a maximum of only 90.39% is achieved by varying the α value of VCE-weight net without the prior [13]. This analysis illustrates the advantage of including the shape prior in extracting desired boundaries.

Figures 4e and 4f show the segmented boundaries of the endocardial and epicardial surfaces of a LA in an example slice from an LGE-MRI image. Together, these two surfaces define the extent of the LA wall and were compared with manual segmentations from experts at the CARMA Center. Average Dice coefficients in this analysis include 0.89 and 0.87 for the epi- and endocardial boundaries in the pre-ablation images, respectively, and 0.87 and 0.86 for the epi- and endocaridal boundaries in the post-ablation images. The histogram plots of Dice measures on endo- and epicardial surfaces in the pre- and post ablated studies are shown in Figure 4g and 4h respectively. We also computed Hausdorff distances to the ground-truth, which provides more insight into the accuracy of both the *shape* and the *local alignment* of our automatic segmentations. For the pre-ablation surfaces, we found an average Hausdorff distance of $1.89 \pm 0.58mm$ and $1.91 \pm 0.55mm$ for epi and endocardium. For the post-ablation surfaces, average distances were $2.36 \pm 0.56mm$ and $2.45 \pm 0.56mm$ for epi- and endocardium, respectively. These errors are consistent with manual segmentation variability reported by CARMA expert segmenters in LGE-MRI images of similar quality.

[2]Our algorithm converges in $\sim$7 iterations on average.

4. REFERENCES

[1] Marrouche, N.F., Wilber, D., Hindricks, G., Jais, P., Akoum, N., Marchlinski, F., Kholmovski, E., Burgon, N., Hu, N., Mont, L., et al.: Association of atrial tissue fibrosis identified by delayed enhancement mri and atrial fibrillation catheter ablation: The decaaf study. JAMA **311**(5) (2014) 498–506

[2] Cootes, T., Taylor, C., Cooper, D., Graham, J.: Active shape models-their training and application. Computer Vision and Image Understanding **61**(1) (1995) 38 – 59

[3] Cootes, T.F., Edwards, G.J., Taylor, C.J.: Active appearance models. PAMI **23**(6) (Jun 2001) 681 – 685

[4] Cremers, D.: Dynamical statistical shape priors for level set-based tracking. PAMI **28**(8) (aug. 2006) 1262 –1273

[5] Malcolm, J., Rathi, Y., Tannenbaum, A.: Graph cut segmentation with nonlinear shape priors. In: ICIP. Volume 4. (16 2007-oct. 19 2007) IV –365 –IV –368

[6] Boykov, Y., Jolly, M.P.: Interactive graph cuts for optimal boundary amp; region segmentation of objects in n-d images. In: ICCV. Volume 1. (2001) 105 –112 vol.1

[7] Gorelick, L., Schmidt, F.R., Boykov, Y.: Fast trust region for segmentation. In: CVPR, 2013 IEEE Conference on, IEEE (2013) 1714–1721

[8] Delong, A., Boykov, Y.: Globally optimal segmentation of multi-region objects. In: Computer Vision, 2009 IEEE 12th International Conference on, IEEE (2009) 285–292

[9] Schmidt, F.R., Boykov, Y.: Hausdorff distance constraint for multi-surface segmentation. In: Computer Vision–ECCV 2012. Springer (2012) 598–611

[10] Wu, X., Chen, D.Z.: Optimal net surface problems with applications. In: Proc. Int. Colloquium on Automata, Languages and Programming. (2002) 1029–1042

[11] Li, K., Wu, X., Chen, D., Sonka, M.: Globally optimal segmentation of interacting surfaces with geometric constraints. In: CVPR. Volume 1. (2004) I–394 – I–399

[12] Song, Q., Bai, J., Garvin, M., Sonka, M., Buatti, J., Wu, X.: Optimal multiple surface segmentation with shape and context priors. TMI IEEE **32**(2) (Feb 2013) 376–386

[13] Veni, G., Fu, Z., Awate, S.P., Whitaker, R.T.: Bayesian segmentation of atrium wall using globally-optimal graph cuts on 3d meshes. In: IPMI, Springer (2013) 656–667

[14] Leventon, M.E., Grimson, W.E.L., Faugeras, O.: Statistical shape influence in geodesic active contours. In: CVPR. Volume 1., IEEE (2000) 316–323

[15] Ishikawa, H.: Exact optimization for markov random fields with convex priors. PAMI **25**(10) (oct. 2003) 1333 – 1336